Raza Moshwan[a,b], Rahmat Firman[a,b], Farazila Yusof[a,b], Mohsen A. Hassan[a,b,c], Mohd Hamdi[a,b], Mohd Fadzil[a,b]

[a]Department of Mechanical Engineering, University of Malaya, Kuala Lumpur, Malaysia
[b]Centre of Advanced Manufacturing and Material Processing (AMMP Centre), University of Malaya, Kuala Lumpur, Malaysia
[c]Department of Mechanical Engineering, Assiut University, Egypt

Dissimilar friction stir welding between polycarbonate and AA 7075 aluminum alloy

In this paper, the effects of process parameters, such as the tool rotational and traverse speeds, on temperature evolution and the microstructural and mechanical properties of dissimilar friction stir welding between 3 mm thick AA 7075 aluminum alloy and polycarbonate (PC) plates were investigated. The tool rotational and traverse speeds were varied from 3000 to 3500 rpm and 50 to 150 mm min^{-1}, respectively. The joint fabricated at 3250 rpm and 100 mm min^{-1} yielded a highest tensile load of 586 N. Microstructural analysis on the stir zone revealed an interlock phenomenon, the transportation of AA 7075 in polycarbonate, and the absence of ceramic-type (carbide, hydride or oxide) compounds. Microhardness (HV) measurement on the weld zone showed an uneven distribution due to the complicated microstructure of the welded joint. The maximum temperatures of 164 °C and 66 °C were obtained at 3250 rpm and 100 mm min^{-1} at a distance of 5 mm away from the welding centerline in the AA 7075 and PC side, respectively.

Keywords: Friction stir welding; AA 7075; Polycarbonate; Mechanical interlocking

1. Introduction

Metals and plastics are extensively used in the manufacturing industry to produce automobile components, electronic devices, and aircraft. Demands for the utilization of lightweight materials such as thermoplastics and aluminum alloys have increased in recent years to reduce the weight of products without sacrificing its structural strength [1]. In addition, polymers offer more flexibility in design, improved thermal insulation properties, and easier manufacturability, which are the key factors in cost saving. Furthermore, governments recently have imposed strict emission laws, such as the European Emissions Standards for new vehicles sold in EU member states, to help reduce pollution. Thus, there is an increasing trend for using lightweight materials in vehicle production, for example the amount of plastic (i.e., lightweight materials) in an average family car has increased from 6% to 15% in the last two decades [2].

Both thermoplastic and aluminum alloys offer high degrees of design freedom and process ability. However, their usage in more complex and larger components is limited to mechanical fasteners and adhesive bonding techniques, processes that possess their own inherent limitations. New joining techniques have been proposed over the years for dissimilar polymer–metal structures [3–5]. Solid-state joining techniques have been proposed for dissimilar material joining, such as friction welding [6, 7], friction spot joining (FSpJ) [4, 8–11], friction stir spot welding (FSSW) [1, 5, 12–15], and friction stir welding (FSW) [16–20]. Although there have been several studies carried out on FSW of dissimilar metals for past few years, the research on FSW of dissimilar materials such as polymer–metal is still in its infancy.

FSW is a solid state joining technique that uses a mechanical stirring process to blend two adjacent materials at the molecular level. This solid state joining process, patented by the Welding Institute (TWI) [21], has induced strong plastic deformation of the weld materials [22] and has already been proven to be a much better joining method with regard to reducing the presence of distortions and residual stresses that plague conventional welding techniques [23]. The technique is currently used for high performance structural applications such as the joining of aerospace components. The microstructural evolution, mechanical properties, and thermal distribution strongly depend on the process parameters that lead to a wide range of possible performances [20, 22, 24, 25].

Lately, the joining of hybrid materials has attracted interest from manufacturers due to their ability in combining the desired mechanical and thermal properties. Recent literature on FSpJ in dissimilar polymer–metal systems, such as hybrid fiber reinforced polymer–magnesium [4] and AA 5052 aluminum alloy–polyethylene terephthalate (PET), have been reported [8]. Furthermore, FSpJ and FSSW have been successfully applied to join high density polyethylene (HDPE) [26–28], polypropylene (PP) [29–32], polymethyl methacrylate (PMMA) sheets [5, 9], and acrylonitrile butadiene styrene (ABS) [5, 33]. This technique was also used to join similar materials such as aluminum alloys [22, 34–37], dissimilar materials with extremely different mechanical, physical, and thermal properties such as aluminum–steel [38–40], aluminum–magnesium [41, 42], aluminum–copper [43–45], and aluminum–titanium [20, 46, 47].

In FSW, considerable changes occur in the microstructure of different areas of the welded zone that can be easily obtained due to the severe strain rates and thermal cycles. In this regard, Grujicic et al. [48] reported a comprehensive modeling of material microstructural evolution during the

FSW of AA 5083 alloy. Their research has resulted in a significant improvement in the relationship between the computed and measured post-FSW residual stress and the material strength distribution. In another paper, a comprehensive fully coupled thermomechanical finite element computation of friction FSW of a prototypical solid-solution strengthened and strain-hardened aluminum alloy (AA 5083) was investigated by Gruijicic et al. [49]. All these works have significantly helped in understanding the modeling of FSW.

Most of the FSW studies have focused on the effect of tooling materials and processing parameters on the mechanical and microstructural properties of the dissimilar metal–metal pairs. However, few studies have been performed on FSW of polymer–metal pairs. Thus, the purpose of this paper is to evaluate the joining performance of FSW between AA 7075 aluminum alloy and polycarbonate (PC) plates in a butt-joint configuration; it also clearly demonstrates the effects of process parameters such as tool rotational and traverse speeds on temperature evolution, and the mechanical and mircostructural properties of the resultant welded joints.

2. Experimental procedure

A schematic diagram of the experimental setup for this study is shown in Fig. 1. A conventional computer numerical control (CNC) high speed milling machine (MITSUI SEIKI model VT3A) was used for the FSW process. Both AA 7075 and PC specimens were prepared in plate form with dimensions of 50 mm × 20 mm × 3 mm. The chemical composition of AA 7075 is shown in Table 1, while the thermo-physical and mechanical performance of the base materials is shown in Table 2. The process parameters used for the experiment are shown in Table 3. During the experiment, the AA 7075 plate was always placed at the advan-

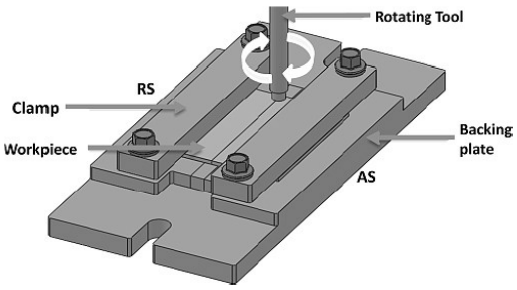

Fig. 1. Schematic diagram of experimental setup in the friction stir butt welding process.

Table 1. Chemical composition of AA 7075 (wt.%) specified by ASM.

Materials	Al	Cr	Cu	Fe	Mg	Mn	Si	Ti	Zn	Other
AA7075	Bal.	0.18–0.28	1.2–2.0	< 0.5	2.1–2.9	< 0.3	< 0.4	< 0.2	5.1–6.1	<0.15

Table 2. Thermo-mechanical performance of the materials used (AA 7075 and PC).

Materials	Yield strength (MPa)	Ultimate Tensile Strength (MPa)	Modulus of Elasticity (GPa)	Elongation at Yield (%)	Elongation at Brake (%)	Glass Transition Temperature, T_g (°C)	Melting Point (°C)
PC	40.7	53	2.48	4.73	63.9	150	267
AA7075	103.0	228	71.70	–	10.5	–	625

Table 3. Summaries of process parameters used in the experiment and tensile load for nine experiments.

Exp. No.	Rotational Speed (rpm)	Traverse Speed (mm min^{-1})	Tensile Load (N)			
			Test 1	Test 2	Test 3	Mean
1	3000	50	273.11	226.21	302.84	267.39
2	3000	100	361.70	417.33	278.78	352.60
3	3000	150	453.88	491.08	427.42	457.46
4	3250	50	374.62	400.56	426.11	400.43
5	3250	100	599.83	554.40	603.80	586.01
6	3250	150	82.76	431.19	388.40	300.79
7	3500	50	340.57	377.24	428.11	381.97
8	3500	100	365.08	248.42	317.92	310.47
9	3500	150	546.68	322.85	443.05	437.53

cing side of the welding tool for a stronger material, as recommended by previous studies [16, 42] while the PC plate was placed on the retreating side.

A hardened tool steel (Fig. 2), was used to produce the welding joints. The tool had a shoulder diameter of 9 mm and probe diameter of 1 mm with 25° taper. The temperature profile during the FSW process was recorded at 10 different locations along the transverse section of the joint evenly distributed on both the AA7075 and PC sides. The arrangement of the K-Type spot weld thermocouples is shown in Fig. 3, which was connected to a DAQ system.

Standard metallographic techniques were used to analyze the resultant joined specimens. Cross-sections of the welded joints were progressively ground using different grades of emery paper, and finally polished using diamond paste (6, 3 and 1 μm) and 0.3 micron alumina. The microstructure of the welded joint was evaluated using an optical microscope (model: Olympus) and a scanning electron microscope (SEM; model: Quanta 2000). Elemental characterization was conducted using energy dispersive X-ray spectroscopy (EDS) and the fracture surfaces in the welded joints were analyzed using X-ray diffraction (Siemens, D5000). Cu-K_α radiation was used in the X-ray diffraction analysis. Mechanical testing of the specimens included tensile tests and hardness measurements; the tensile tests were carried using an Instron universal testing machine with a load cell system (model 3369). To find the average tensile strength, three parallel tests were carried for each combination of parameters (Table 3). The hardness in the welded area was measured using a Vickers micro indentation device (Shimadzu, HMV 2T E) with a 0.025 N load and a 5 sec holding time for the PC side and a 0.2 N load with the same holding time for AA 7075 side.

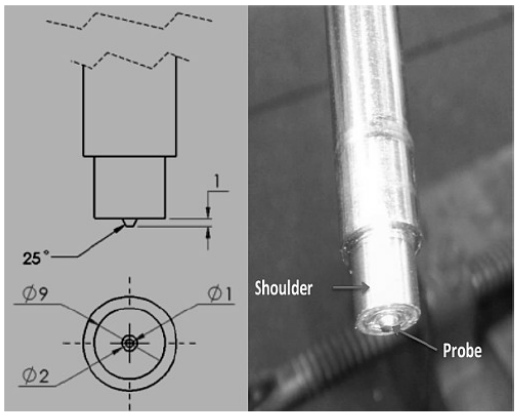

Fig. 2. Tool dimensions and structure.

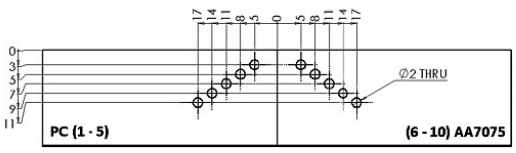

Fig. 3. Schematicr diagram of ten holes for thermocouple attachment (in mm).

3. Results and discussion

3.1. Tensile strength analysis

A representative surface appearance of the welded joint at 3500 rpm and 50 mm min^{-1} is shown in Fig. 4. The influence of the tool rotational and traverse speeds on the tensile strength and elongation of the friction stir welded joints is shown in Fig. 5. As shown in Fig. 5, at 3250 rpm with the increase of traverse speed the tensile load increases while it is inconsistent at 3000 and 3500 rpm. A highest tensile load of 586 N was obtained at 3250 rpm and 100 mm min^{-1}, while the lowest value of 310 N can be obtained at 3500 rpm and 150 mm min^{-1}.

It is well known that similar welds are structurally weaker than dissimilar welds regardless of the type of material used. However, in the case of PC–AA 7075 welded joints, a very low tensile load was obtained in which the ultimate tensile strength (*UTS*) of the welded joint was less than 10 % of the PC base material. Payganeh et al. [50] reported similar results for the FSW of polypropylene (PP) in which the *UTS* of similar PP welded joint was only 10–25 % of the *UTS* of the PP base material. In addition, the EDX mapping and spot analyses proved that no significant mixture occurred between polycarbonate and AA 7075, and no second phase particles were formed.

In the welding process, the heat input plays an important role in the tensile properties and hardness of the welded joints. The specific weld input energy for FSW is greatly influenced by tool rotational and traverse speeds. In general, increase in the rotary speed of the tool will generate more

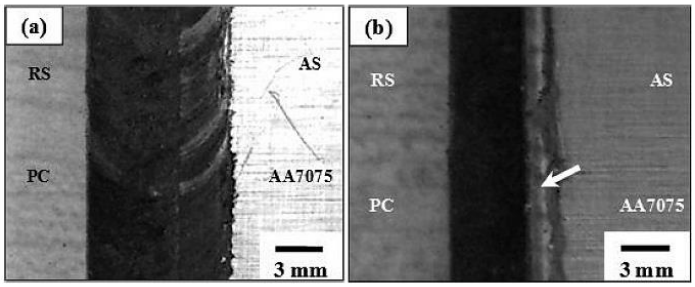

Fig. 4. Surface appearances of the welded joint at 3500 rpm and 50 mm min^{-1} (a) front side (b) rear side.

frictional heating and greater mechanical stirring. Increasing the welding temperature increases the plastic softening and liquidity of the weld material, which improves the weld quality. At the same time, large plastic deformation enhances the strain strengthening effect and improves the joint strength.

In general, in the case of FSW of metallic material, the joint experiences more intense stir and friction heat toward the bottom of the weld, and the large plastic deformation increases the dislocation concentration. Meanwhile, the higher temperature strengthens the interactions between the dislocations and those between the dislocations and other crystalline imperfections that increase the resistance force to the dislocation motion. Therefore, the piling effect of dislocations in the weld top is much weaker than that in the bottom during the tensile test. However, in our current study we observed more transportation of AA 7075 in PC than dislocation which caused mechanical interlocking between these two materials and ultimately enhanced the strength of the welded joint.

3.2. Hardness analysis

The value of Vickers microhardness at the joint interface on the PC side at a distance of 1 mm up to 5 mm from the welding center line is shown in Fig. 6. As shown in Fig. 6, when the distance from the welding centerline increases, the hardness increased. The lowest hardness value of 6.6 $HV_{0.025}$ was obtained at 1 mm on the PC side. The hardness sharply increased from 6.6 $HV_{0.025}$ to 11.3 $HV_{0.025}$ for the range from 1 to 1.5 mm, and then increased gradually to 12.7 $HV_{0.025}$, which is an indication of the hardness of the PC base material as it is reached at 5 mm from the welding centerline on the PC side.

The value of Vickers microhardness at the joint interface on the AA 7075 side was measured at a distance from 0.75 to 5 mm from the welding center line shown in Fig. 7. The lowest value of hardness, 120 $HV_{0.2}$, was obtained at 0.75 mm. The hardness then increased up to 160 $HV_{0.2}$ at 0.5 mm from the welding center line. Subsequent readings of the hardness indicated a stable range of 154–162 $HV_{0.2}$ which was an indication of the hardness of the AA 7075 base material. The hardness reduction was clearly observed in the welded area of the PC side, caused by thermal degra-

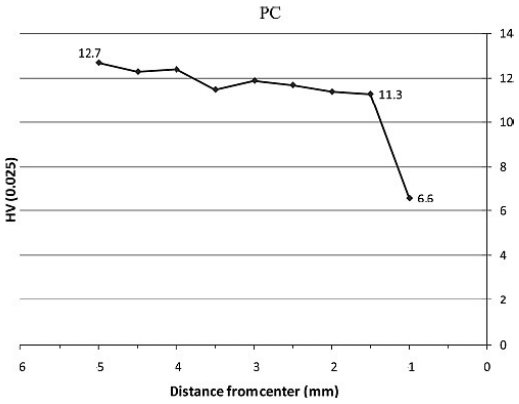

Fig. 6. Vickers microhardness at PC joint interface.

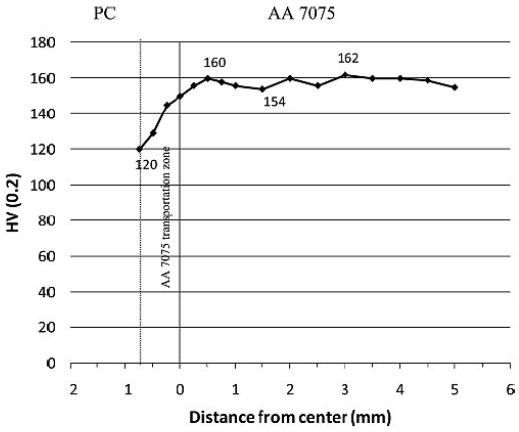

Fig. 7. Vickers microhardness at AA7075 base material and AA 7075 transportation interface.

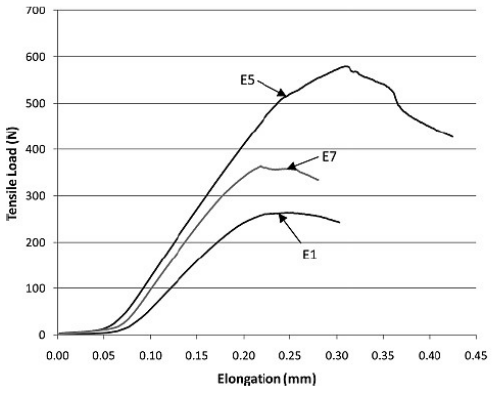

Fig. 5. Tensile load curve for highest, middle, and lowest load for E5, E7, and E1, respectively.

Link to Full-Text Articles:

http://repository.um.edu.my/94858/1/Journal%20of%20Material%20Research.pdf